J. Fluid Mech. (1973), *vol.* 60, *part* 3, *pp.* 513–538
Printed in Great Britain

Fluid flow around and through a screen

By J.-K. KOO AND DAVID F. JAMES
Department of Mechanical Engineering, University of Toronto

(Received 17 July 1972 and in revised form 21 March 1973)

A mathematical model is proposed for steady two-dimensional flow around a submerged screen. The general problem analysed is the flow in a parallel-sided channel partially spanned by a screen, and the fluid is considered to be inviscid except at the screen, where the flow has the required pressure drop. The model is constructed by first replacing the screen with a distribution of sources and then manipulating the stream function for this flow so that the mass and momentum balances across the screen are satisfied. Consequently the model predicts a flow field which is realistic except for the expected discontinuity in velocity between the wake and external flow. In general, the governing equations must be solved numerically, but for the important case of a plane screen oriented normal or roughly normal to the approaching flow, an approximate analytical solution is possible. The accuracy of the model was ascertained by conducting wind-tunnel tests on screens of various solidities and orientations, and comparing the measured downstream velocity distributions with those predicted by the numerical and analytical solutions of the model. Overall, the theoretical results agree well with the experimental data, showing that the model is valid for screens of low and high solidity, in fact, for pressure drop coefficients up to 10. Comparisons with the work of others show that the proposed model is also accurate for the special cases of a screen submerged in an infinite flow field and of a screen spanning the full width of the channel.

1. Introduction

When fluid passes through a screen or gauze, the flow is altered in two ways: the static pressure is reduced and the streamlines are deflected towards the normal to the screen. The reduction in pressure is usually expressed by the dimensionless pressure drop coefficient K, defined as $K = \Delta p / \frac{1}{2}\rho V^2 \cos^2\theta$, where Δp is the pressure drop, ρ the fluid density, V the magnitude of the fluid velocity and θ the angle of incidence, i.e. the angle between the oncoming streamline and the normal to the screen. The coefficient K is of course a measure of the screen solidity (Baines & Peterson 1951), and generally depends on the velocity. However, the experiments of Schubauer, Spangenberg & Klebanoff (1950) have shown, for screens of various solidities, that K is velocity-independent when the normal component $V\cos\theta$ is sufficiently large. This feature is analogous to, and in fact related to, the constancy of the drag coefficient at sufficiently large Reynolds numbers for the flow around submerged bodies. The second change in the flow, the deflexion of the streamlines, is generally expressed by the deflexion coefficient

D_θ, defined as the ratio of the tangential velocity after the screen to that before. Taylor & Batchelor (1949) showed that

$$D_\theta = \frac{2\theta}{\sin 2\theta} \frac{1{\cdot}1}{[1 + K\cos^2\theta]^{\frac{1}{2}}} + 1 - \frac{2\theta}{\sin 2\theta}.$$

For small θ, this equation reduces to $D_\theta = 1{\cdot}1/(1+K)^{\frac{1}{2}}$, which is a well-known and useful approximation, particularly since D_θ is a function of K only.

The first comprehensive analysis of flow through screens was carried out by Taylor & Batchelor (1949). They were primarily interested in showing how turbulence intensity is reduced when the fluid passes through a screen, and to this end studied the case of a channel flow in which a non-uniform stream passed through a flat screen perpendicular to the channel walls. Their analysis showed that a small non-uniformity in the approaching velocity profile is attenuated by a factor depending on K and θ/ϕ, where ϕ is the angle between the outgoing streamline and the normal to the screen. Later Elder (1959) treated the more general case of an arbitrarily shaped and non-uniform screen in a two-dimensional channel flow. By linearizing the matching conditions at the screen, Elder obtained a linear relation between the upstream velocity profile, the downstream profile, the shape of the screen and the variation of K along the screen; hence any one of these four quantities can be solved for in terms of the other three. Elder's analysis and the accompanying experiments were for screens occupying the full cross-section of the channel, but he mentioned in passing that his technique could also be applied to partial screens (occupying a portion of the cross-section) providing $K \ll 1$. This is one of the first references to the problem of a partial screen, and our paper will later show that Elder's technique cannot properly be applied to this case; however, even if improperly applied, the predictions from his linearized theory provide a good approximation for values of K up to 1. A method of treating the problem of a finite plane screen in an infinite flow field was proposed in some early work by Küchemann & Weber (1953). They modelled the flow by superposing two vortex distributions, one along the screen and the other along the wake boundary, on a uniform flow. Their method appears to be difficult to employ when dealing with a partial screen, because the vortex strengths and boundary location are not known *a priori* and must be found by trial and error. The technique, however, has been successfully applied to flow through a cooler block in a diffuser (physically similar to a sheet of honeycomb at the end of a smooth expansion in a duct), where the problem is tractable because the direction of the downstream flow is fixed by the duct and by vanes within the cooler block. Another solution for a full screen inside a duct was recently put forward by Lau & Baines (1968), who solved for the screen shape corresponding to specified upstream and downstream velocity profiles for a stratified two-dimensional flow in a straight duct. Their solution, which predicts the curvature of the screen, requires that the local inclination of the screen be everywhere small.

A different type of screen problem, with a different analytical approach, was treated by Taylor (1963). Taylor considered the case of a screen submerged in an infinite two-dimensional flow field, and his method of solution consisted of re-

placing the screen by uniformly distributed sources, which when combined with the approaching flow produced a realistic flow field and generated a prediction of the screen drag coefficient in terms of K. In his solution, continuity through the screen is not satisfied and consequently only the flow field outside the wake can be determined. As will be shown later in this paper, Taylor's solution is a good approximation if K is limited to small values.

As the above review suggests, most known solutions of screen flows are perturbation solutions, generally limited to small deviations from parallel flow and/or to small values of K; also, most known methods are for situations where the screen spans the entire cross-section of the flow. The objective of the present work is to find the general solution for two-dimensional flow around and through a partial screen in a straight channel; hopefully the solution will be valid for the full range of K, and will include the special cases of a full screen in a confined flow and a finite screen in an infinite flow field. The approach taken here is not to solve the governing equations directly, but rather to formulate a mathematical model which satisfies the governing equations and the most important boundary conditions.

The problem studied in this paper is a real one, since it pertains to numerous practical situations in which flow passes partly through and partly around a porous body; common examples of such bodies are parachutes, fish nets, natural and artificial wind breaks and the slotted injection disks in oil combustion chambers, which are used to create a low-velocity zone suitable for ignition. The results presented herein can be used to determine the surrounding velocity field, especially in the important wake region, and to estimate the drag force on the porous body.

2. A mathematical model

When a screen partially fills the cross-section of a channel, the velocity field may be conveniently divided into two distinct regions, one outside and the other inside the wake. These regions are designated I and II respectively in figure 1, which shows the general pattern for the two-dimensional flow and which also defines some of the parameters of the problem; the screen, designated by a series of dots in the diagram, is an arbitrarily curved sheet of height λ. It is assumed throughout the analysis that the fluid is inviscid in both regions except in the immediate neighbourhood of the screen; thus Bernoulli's equation applies along all streamlines in the flow field, but not across the screen. For a uniform flow far upstream, the flow is irrotational in region I, while in the wake region the flow will generally be rotational because of non-uniform energy losses along the screen. Consequently, $\nabla^2\psi_{\mathrm{I}} = 0$ is the governing equation for the stream function in region I and $\nabla^2\psi_{\mathrm{II}} = f(\psi_{\mathrm{II}})$ holds in region II, where f is an unknown function representing the vorticity generated at the screen. Regions I and II are separated by the streamline AC, which passes through the tip A of the screen, and across which there is a theoretical step change in the velocity.

To construct the mathematical model, the screen is first imagined as a continuous distribution of sources. When the flow from the source distribution is

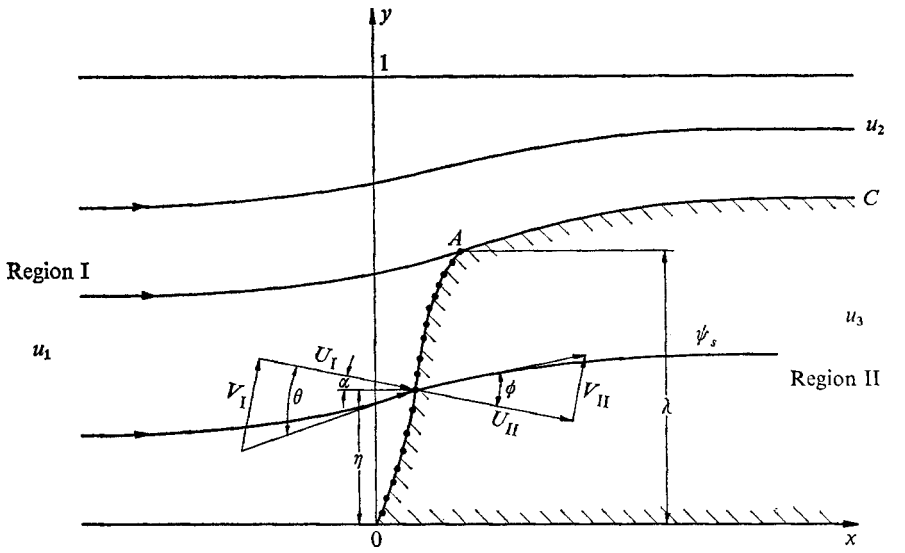

FIGURE 1. General features of two-dimensional flow around and through a screen in a channel. The diagram also defines some of the variables in the analysis.

added to the approaching channel flow, the resulting pattern is very similar to that shown in figure 1. Let $\psi(x, y)$ represent the stream function for these combined flows, where x and y are Cartesian co-ordinates having their origin at the base of the screen. The essence of the present technique is to set ψ_{I} equal to ψ in region I and then to require that the streamline pattern for ψ_{II} be the same as that for ψ in region II; that is, if u and v represent the horizontal and vertical velocity components respectively, then we require that $v_{\mathrm{II}}/u_{\mathrm{II}} = v/u$, or that

$$\frac{-\partial\psi_{\mathrm{II}}/\partial x}{\partial\psi_{\mathrm{II}}/\partial y} = \frac{-\partial\psi/\partial x}{\partial\psi/\partial y}.$$

This stipulation is satisfied by $\psi_{\mathrm{II}} = g(\psi)$ in general, but the particular form which is convenient for our purposes is $\psi_{\mathrm{II}} = B(\psi)\,\psi$. By this representation, $B(\psi)$ may be considered an attenuation function, with values between 0 and 1. The upper limit is approached as $K \to 0$ and the screen effectively vanishes; the lower limit is realized when $K \to \infty$ and the screen becomes a solid plate with no flow behind it. Consequently, the stream function of the combined flows is not by itself the solution of the problem; rather, it acts as the basic function on which the model is constructed.

Since the attenuation function $B(\psi)$ does not change the streamline shape, the flow patterns for regions I and II fit together exactly along the dividing streamline AC (figure 1). However, it is easy to show that the static pressure is not continuous across AC. The difference depends on the variation of velocity along the streamline, but as Koo has shown in his (1971) thesis, AC is very nearly a free streamline since the velocity along it is within 2 % of being constant, except in the immediate neighbourhood of the screen tip, where it becomes infinite owing to the logarithmic singularity of the source flow there. Consequently, the

model produces a discontinuity in pressure between regions I and II, but this fortunately turns out to be small.

One of the unknowns in the present problem, then, is $B(\psi)$, and it will be shown in the forthcoming analysis that the other unknown is the strength distribution of the sources; these two unknowns will be found by satisfying mass and energy balances across the screen.

3. The source solution

The first step of the method is to find ψ, the stream function for an arbitrary but continuous distribution of sources in an approaching uniform inviscid flow. Let the location of the screen OA be designated by the equation $\xi = g(\eta)$, where ξ and η are the co-ordinates of the screen in the x and y directions respectively, as shown in figure 2; since λ is the projected height of the screen, $0 \leqslant \eta \leqslant \lambda$. The function $g(\eta)$ is assumed to be known and single-valued, and in complex notation the screen may be represented by the single variable $\zeta = \xi + i\eta$. The source strength per unit length along the screen may then be denoted by $\gamma(|\zeta|)$, and in order to find the two-dimensional potential flow field generated by γ within a channel, the method of images is employed. The lower wall $y = 0$ is removed by adding a source distribution, denoted by OA' in figure 2, to the original distribution making the total distribution symmetric. The combined distribution $A'OA$ is then repeated on the horizontal lines $y = \pm 2, \pm 4, \pm 6$, etc., as illustrated in the figure. Accordingly, the entire source system may be represented by the equation

$$\zeta_n(\eta) = g(|\eta|) + i(\eta + 2n), \quad -\lambda \leqslant \eta \leqslant \lambda \quad (n = 0, \pm 1, \pm 2, \ldots).$$

To construct the potential function Ω for this system of images, consider the infinite series of points $\zeta_n(\eta_0)$, $-\lambda \leqslant \eta_0 \leqslant \lambda$, located two units apart along the vertical line $\xi_0 = g(\eta_0)$. At each point, an infinitesimal distance along the curve ζ_n is represented by $|d\zeta_n|$, so that the source strength there is $\gamma(|\zeta_n|)\,|d\zeta_n|$. It is shown in Robertson (1965, p. 136) that the complex potential function for an infinite number of sources equally spaced two units apart and each of strength $\gamma(|\zeta|)\,|d\zeta|$ is

$$\frac{\gamma(|\zeta|)\,|d\zeta|}{2\pi} \ln \sin \frac{\pi(z-\zeta)}{2i},$$

where z is the standard complex variable $x + iy$. Since this function represents the contribution from a segment of the source distribution, the potential function $\Omega(z)$ for the entire source system is found by integrating along the source line from A' to A; that is,

$$\Omega(z) = \int_{\zeta(-\lambda)}^{\zeta(+\lambda)} \frac{\gamma(|\zeta|)}{2\pi} \ln \sin \frac{\pi(z-\zeta)}{2i}\,|d\zeta|,$$

where $\zeta(\pm\lambda) = g(\lambda) \pm i\lambda$. If $g(\eta)$ is a single-valued function and if η is made the variable of integration in the above integral, then

$$\Omega(z) = \int_{-\lambda}^{\lambda} \frac{\Gamma(|\eta|)}{2\pi} \ln \sin \frac{\pi[z - (g(|\eta|) + i\eta)]}{2i}\,|d\eta|,$$

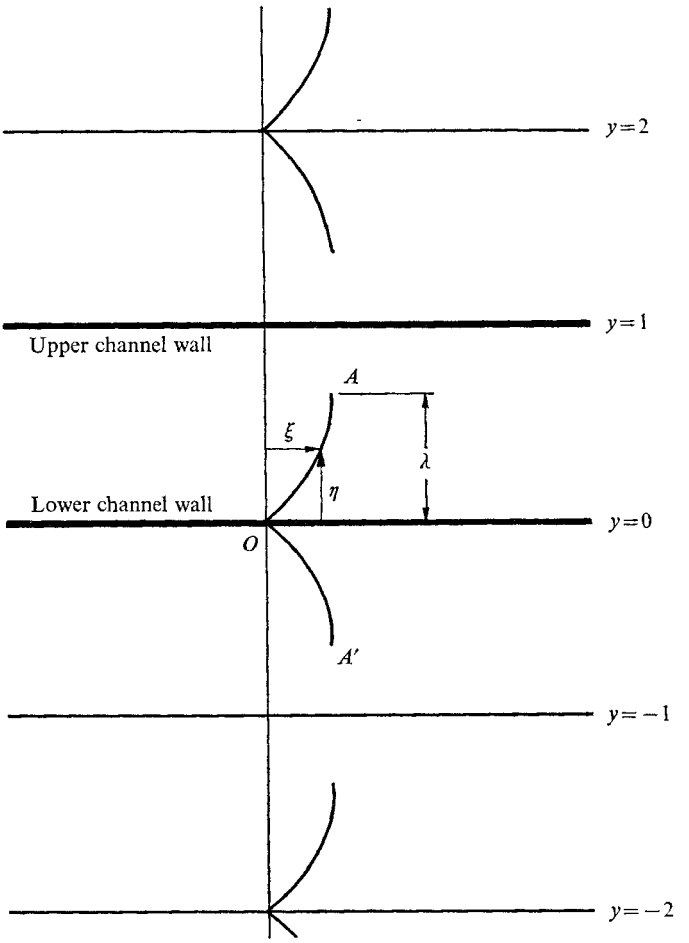

FIGURE 2. The arrangement of images for the source distribution.

in which $\Gamma(|\eta|)$ has been substituted for $\gamma(|\zeta|)\,[(dg/d\eta)^2+1]^{\frac{1}{2}}$. The modulus sign around η may be removed by rewriting:

$$\Omega(z) = \int_0^{\lambda} \frac{\Gamma(\eta)}{2\pi} \ln \sin \frac{\pi}{2i}\,[z-(g(\eta)+i\eta)]\,d\eta + \int_0^{\lambda} \frac{\Gamma(\eta)}{2\pi} \ln \sin \frac{\pi}{2i}\,[z-(g(\eta)-i\eta)]\,d\eta.$$

To this is added $z+c$, the complex potential for the approaching uniform flow (the velocity of the uniform stream has been set equal to 1 without loss of generality); thus the stream function ψ is given by

$$\psi(x,y) = \operatorname{Im}[\Omega(z)+z+c].$$

According to the procedure set out earlier, the stream functions for regions I and II are

$$\psi_{\mathrm{I}}(x,y) = \psi(x,y), \quad \psi_{\mathrm{II}}(x,y) = B(\psi)\,\psi(x,y).$$

ψ_{I} satisfies Laplace's equation and the boundary conditions on the walls in region I; ψ_{II} satisfies the boundary condition on the lower wall and matches with ψ_{I} along the dividing streamline. Since the only unknown in ψ is the function $\Gamma(\eta)$, ψ_{I} and ψ_{II} are given in terms of the two unknowns $\Gamma(\eta)$ and $B(\psi)$.

4. The matching conditions

The two unknowns can be found from two matching conditions at the screen. The first condition is that the velocity U normal to the screen be continuous across the screen; that is, at any point η on the screen

$$U_{\mathrm{I}}(\eta) = U_{\mathrm{II}}(\eta), \tag{1}$$

where the subscripts continue to refer to regions I and II.

The second matching condition starts with the relation for the pressure drop across the screen $\Delta p(\eta) = \frac{1}{2}K\rho U_{\mathrm{I}}^2(\eta)$.

Using this relation in conjunction with Bernoulli's equations on a streamline outside the wake and on the two segments of the streamline $\psi = \psi_s$ passing through η, the following energy equation can be derived, and is the second matching condition:

$$KU_{\mathrm{I}}^2(\eta) = u_2^2 - u_3^2(\psi_s) + V_{\mathrm{II}}^2(\eta) - V_{\mathrm{I}}^2(\eta), \tag{2}$$

where u_2 and u_3 are the far-downstream velocities in region I and on ψ_s respectively, and V_{I} and V_{II} are the tangential velocities on each side of the screen (figure 1). The far-upstream velocity u_1 is assumed to be uniform. The six velocities in (1) and (2) can be found from ψ_{I} and ψ_{II}, and will be functions of $\Gamma(\eta)$ and $B(\psi)$; accordingly, substitution of the velocities will yield two equations for the two unknowns Γ and B. Before attempting to solve for Γ and B, it should be noted that we have not attempted to satisfy the deflexion condition at the screen. This shortcoming will be discussed later in the paper, and for the moment we recognize that its inclusion would overspecify the problem for Γ and B.

Solutions of the problem for plane screens will be discussed in three sections: (i) an analytical solution for a normal (i.e. perpendicular) screen, in which certain approximations are made but the resulting errors appear to be very small, (ii) an analytical solution for an inclined screen, which can be achieved only by further approximations and with a consequent loss in accuracy, and (iii) a numerical solution for normal and inclined screens, which retains all terms and thereby provides solutions by which the accuracy of the analytical solutions may be gauged.

5. Solutions for plane screens

5.1. *An analytical solution for a normal screen*

This section will show that, if the tangential velocities in the second matching equation are neglected, then the source distribution is uniform, in which case the flow field is readily determined. We start the procedure, however, with the unabridged matching conditions (1) and (2), for which the velocity components U_{I}, U_{II}, u_2, u_3, V_{I} and V_{II} must be determined.

The horizontal velocity component in region I is $u_{\mathrm{I}} = \mathrm{Re}\{d(\Omega + z + c)/dz\}$. Using the previously derived expression for Ω, and setting $g(\eta) = 0$ for a normal screen, yields

$$u_{\mathrm{I}}(x, y) = 1 + \frac{1}{4}\int_0^{\lambda} \Gamma(\eta) \sinh \pi x \left[\frac{1}{\cosh \pi x - \cos \pi(y-\eta)} + \frac{1}{\cosh \pi x - \cos \pi(y+\eta)}\right] d\eta.$$

The corresponding component in region II is

$$u_{\mathrm{II}}(x,y) = \partial\psi_{\mathrm{II}}/\partial y = E(\psi)\,u(x,y),$$

where $E(\psi) = B + \psi\, dB/d\psi$ and $u(x,y)$ has the same mathematical expression as u_{I}. Hence the far-field velocities are

$$u_1 = u_{\mathrm{I}}(-\infty,y) = 1 - \frac{1}{2}\int_0^\lambda \Gamma(\eta)\,d\eta, \tag{3a}$$

$$u_2 = u_{\mathrm{I}}(+\infty,y) = 1 + \frac{1}{2}\int_0^\lambda \Gamma(\eta)\,d\eta, \tag{3b}$$

$$u_3 = u_{\mathrm{II}}(+\infty,y) = E(\psi_s)\left[1 + \frac{1}{2}\int_0^\lambda \Gamma(\eta)\,d\eta\right]. \tag{3c}$$

The components normal to the screen, U_{I} and U_{II}, cannot be found as simply as the above velocities, and in order to proceed straightforwardly in this part of the text, the analysis for these velocities has been set aside in the appendix. The appendix shows that

$$U_{\mathrm{I}} = u_{\mathrm{I}}(0,y) = 1 - \tfrac{1}{2}\Gamma(y), \tag{4a}$$

$$U_{\mathrm{II}} = u_{\mathrm{II}}(0,y) = E(\psi_s)\,[1 + \tfrac{1}{2}\Gamma(y)]. \tag{4b}$$

In the same manner, the vertical velocity in region I is $v_{\mathrm{I}} = \mathrm{Im}\,\{d(\Omega + z + c)/dz\}$,

or
$$v_{\mathrm{I}}(x,y) = \int_0^\lambda \Gamma(\eta)\,p(x,y,\eta)\,d\eta,$$

where
$$p(x,y,\eta) = \frac{1}{4}\left[\frac{\sin\pi(y-\eta)}{\cosh\pi x - \cos\pi(y-\eta)} + \frac{\sin\pi(y+\eta)}{\cosh\pi x - \cos\pi(y+\eta)}\right].$$

Therefore the components tangential to the screen are

$$V_1 = v_{\mathrm{I}}(0,y) = \int_0^\lambda \Gamma(\eta)\,p(0,y,\eta)\,d\eta, \tag{5a}$$

$$V_{\mathrm{II}} = E(\psi_s)\,v_{\mathrm{I}}(0,y). \tag{5b}$$

On substituting for U_{I}, u_2, u_3, V_{I} and V_{II} in (2), the second matching condition becomes

$$K\left[1 - \frac{\Gamma(y)}{2}\right]^2 = [1 - E^2]\left\{\left[1 + \frac{1}{2}\int_0^\lambda \Gamma(\eta)\,d\eta\right]^2 - \left[\int_0^\lambda \Gamma(\eta)\,p(0,y,\eta)\,d\eta\right]^2\right\}. \tag{6}$$

E can be expressed as a function of $\Gamma(y)$ by combining the first matching condition and (4), namely

$$E = (1 - \tfrac{1}{2}\Gamma(y))/(1 + \tfrac{1}{2}\Gamma(y)). \tag{7}$$

Also, if the tangential velocity at the screen is much less than the normal velocity, i.e. if $V_{\mathrm{I}}^2 \ll U_{\mathrm{I}}^2$, then the second integral in (6) can be neglected. By this approximation, (6) is reduced to a relation for $\Gamma(y)$, and since the only other terms appearing in the equation, K and $\int_0^\lambda \Gamma(\eta)\,d\eta$, are both constants, consequently $\Gamma(y)$ is also a constant, say Γ_s. In this case, then, the source strength is uniform over the length of the screen, and given K and λ, Γ_s may be found from the approximate

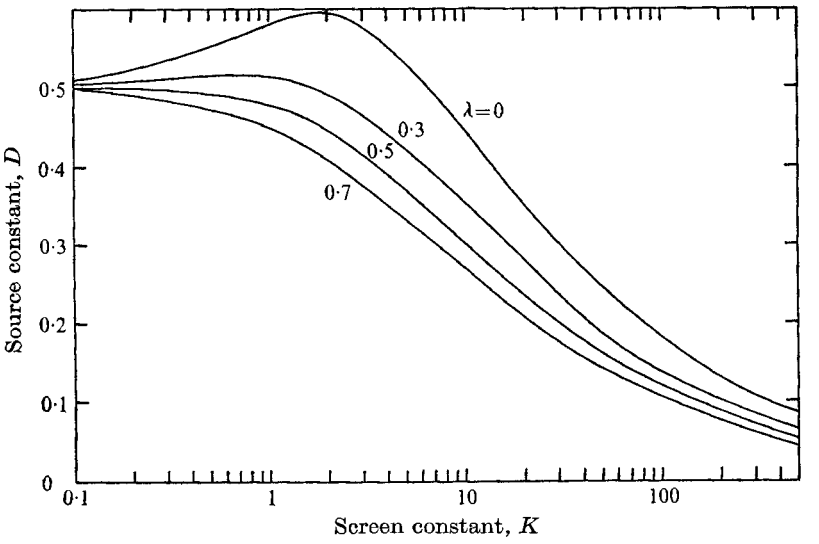

FIGURE 3. The source constant D as a function of the screen coefficient K, for various values of the screen height λ from (8).

form of (6). An equivalent procedure is to follow Taylor (1963) and introduce the source constant D, defined by $\Gamma_s = DKU_1 = 2DK/(2+DK)$. This solution makes D the unknown in (6), and with the V^2 term neglected, the equation becomes

$$K = \frac{2DK+(DK)^2}{(1+DK)^2}\left[1+\frac{DK}{2}(1+\lambda)\right]^2. \tag{8}$$

The solution of this implicit relation is given graphically in figure 3, for various values of K and λ.

Using the substitution for Γ_s, the far-field velocities may be expressed in terms of D, K and λ:

$$u_1 = 1-\frac{\lambda DK}{2+DK},$$

$$u_2 = 1+\frac{\lambda DK}{2+DK},$$

$$u_3 = \frac{1}{1+DK}\left(1+\frac{\lambda DK}{2+DK}\right).$$

The downstream velocity profile, as given by u_2 and u_3, is now known and will be exhibited later in the paper alongside other predicted velocity distributions and experimental data.

Another result which may be computed is the drag coefficient C_D for the screen. Since

$$C_D \equiv \frac{\text{pressure drop}}{\text{upstream kinetic head}} = \frac{\frac{1}{2}K\rho U_1^2}{\frac{1}{2}\rho u_1^2},$$

and since U_1 and u_1 are known in terms of K, D and λ,

$$C_D = \frac{K}{(1+\frac{1}{2}DK)^2[1-\lambda DK/(2+DK)]^2}. \tag{9}$$

This formula correctly yields $C_D = K$ when $\lambda = 1$, and also predicts the drag coefficient of a screen submerged in an infinite flow field, that is, for $\lambda = 0$; this latter prediction will be compared with Taylor's (1963) findings in § 8.

5.2. *An analytical solution for an inclined screen*

For the case of a plane screen inclined at an arbitrary angle to the channel walls, an approximate analytical solution may be found in a manner similar to that for a normal screen. The equation for the screen is now $g(\eta) = a|\eta|$, $-\lambda \leqslant \eta \leqslant \lambda$, where $\alpha = \tan^{-1} a$ is the angle which the oncoming parallel flow makes with the normal to the screen. The horizontal velocity in region I is then

$$u_{\mathrm{I}}(x, y) = 1 + \int_0^{\lambda} \Gamma(\eta)\, H(x, y, \eta)\, d\eta,$$

where $$H(x, y, \eta) \equiv \tfrac{1}{4} \sinh\{\pi(x - a\eta)\} \left[\frac{1}{\cosh \pi(x - a\eta) - \cos \pi(y - \eta)} + \frac{1}{\cosh \pi(x - a\eta) - \cos \pi(y + \eta)} \right].$$

The far-field velocities u_1, u_2 and u_3 are determined from the above equation by letting $x \to \pm\infty$; these are found to be the same as for a normal screen, i.e. they are given by (3). The velocity components on the screen are found by letting $x \to ay \pm$, where the $\pm$ notation indicates whether the approach is from the right $(+)$ or left $(-)$. When $x \to ay \pm$ in $H(x, y, \eta)$, it becomes apparent that H is unbounded as $\eta \to y \pm$ and is small otherwise; moreover, H approaches an impulse function as $a \to 0$. Since a is assumed to be small, and since we wish to proceed with an analytical solution, let $H(ay \pm, y, \eta)$ be approximated by the Dirac delta function $\pm \pi \delta(y - \eta)$, in which the factor π ensures that the integral of H has the required value of unity. With this approximation for H, the horizontal velocity components at the screen are again

$$u_{\mathrm{I}}(ay_-, y) = 1 - \tfrac{1}{2}\Gamma(y),$$

$$u_{\mathrm{II}}(ay_+, y) = E(\psi_s)\,[1 + \tfrac{1}{2}\Gamma(y)].$$

Turning now to the vertical component of velocity in region I,

$$v_{\mathrm{I}}(x, y) = \int_0^{\lambda} \Gamma(\eta)\, P(x, y, \eta)\, d\eta,$$

where

$$P(x, y, \eta) \equiv \frac{1}{4} \left[\frac{\sin \pi(y - \eta)}{\cosh \pi(x - a\eta) - \cos \pi(y - \eta)} + \frac{\sin \pi(y + \eta)}{\cosh \pi(x - a\eta) - \cos \pi(y + \eta)} \right].$$

On the screen, as $x \to ay \pm$,

$$v_{\mathrm{I}}(ay_-, y) = \int_0^{\lambda} \Gamma(\eta)\, P(ay_-, y, \eta)\, d\eta \equiv v(y_-) = v_-,$$

$$v_{\mathrm{II}}(ay_+, y) = E(\psi_s)\, v_{\mathrm{I}}(ay_+, y) \equiv Ev(y_+) = Ev_+.$$

Having found the horizontal and vertical components, the normal and tangential velocities to the screen are

$$U_{\mathrm{I}} = u_{\mathrm{I}}(ay_-, y)\cos\alpha - v_{\mathrm{I}}(ay-, y)\sin\alpha = u_{\mathrm{I}}\cos\alpha - v_-\sin\alpha,$$
$$U_{\mathrm{II}} = u_{\mathrm{II}}(ay_+, y)\cos\alpha - v_{\mathrm{II}}(ay_+, y)\sin_+ = u_{\mathrm{II}}\cos\alpha - Ev_+\sin\alpha,$$
$$V_{\mathrm{I}} = u_{\mathrm{I}}\sin\alpha + v_-\cos\alpha, \quad V_{\mathrm{II}} = u_{\mathrm{II}}\sin\alpha + v_+\cos\alpha.$$

If these expressions are used, (1) becomes

$$E = \frac{(1-\frac{1}{2}\Gamma(y))\cos\alpha - v_-\sin\alpha}{(1+\frac{1}{2}\Gamma(y))\cos\alpha - v_+\sin\alpha} = \frac{1-\frac{1}{2}\Gamma(y) - v_-\tan\alpha}{1+\frac{1}{2}\Gamma(y) - v_+\tan\alpha}$$

and (2) becomes

$$KU_{\mathrm{I}}^2 = (1-E^2)\left[1+\frac{1}{2}\int_0^\lambda \Gamma(\eta)\,d\eta\right]^2 + E^2\left[\left(1+\frac{\Gamma(y)}{2}\right)\sin\alpha + v_+\cos\alpha\right]^2 - \left[\left(1-\frac{\Gamma(y)}{2}\right)\sin\alpha + v_-\cos\alpha\right]^2. \tag{10}$$

If $v_\pm$ is small, i.e. much less than one, then $E \simeq (1-\frac{1}{2}\Gamma)/(1+\frac{1}{2}\Gamma)$ and

$$U_{\mathrm{I}} \simeq (1-\tfrac{1}{2}\Gamma)\cos\alpha.$$

By these approximations, (10) is simplified to

$$K\left[1-\frac{\Gamma(y)}{2}\right]^2\cos^2\alpha = \frac{2\Gamma(y)}{[1+\frac{1}{2}\Gamma(y)]^2}\left[1+\frac{1}{2}\int_0^\lambda \Gamma(\eta)\,d\eta\right]^2,$$

so that $\Gamma(y)$ is again a constant, Γ_s, which is therefore given by the equation

$$K[1-\tfrac{1}{4}\Gamma_s^2]^2\cos^2\alpha = 2\Gamma_s[1+\tfrac{1}{2}\lambda\Gamma_s]^2.$$

When K, α and λ are specified, Γ_s may be found and consequently the velocities u_1, u_2 and u_3 may be calculated. Such calculations have been carried out for a modest variation of the parameters and the results, like those for a normal screen, will be presented later. It should be noted that the above relation makes no distinction between backward- and forward-tilting screens. To be consistent with the approximation that $v_\pm \ll 1$, the solution associated with the above equation is expected to be most useful for small values of α and up to moderate values of K.

5.3. *A numerical solution*

In the previous sections, analytical solutions were possible only by ignoring the vertical component of velocity at the screen. A more general solution did not seem feasible because of the nonlinear nature of the integral equations for $\Gamma(\eta)$, and consequently a numerical technique was devised to solve these integral equations, including the previously neglected terms, and so obtain a more accurate representation of the flow field. A complete description of this technique can be found in Koo's (1971) thesis; although the method is significant in some respects and might deserve more attention, only a brief outline will be presented in this section.

The numerical technique was essentially an iterative scheme to find a function $\Gamma(\eta)$ which satisfied (10) for ten values of η; that is, at ten equally spaced

locations along the screen. This was achieved by assuming an initial distribution for Γ, iterating about that solution to generate an improved estimate for Γ and then continuing the iterations until Γ satisfied (10) to sufficient accuracy. The high-speed computations were carried out for $\lambda = 0{\cdot}5$ and for all combinations of $\alpha = 0$, $\pm 30°$ and $\pm 45°$ and $K = 3{\cdot}0$, $4{\cdot}6$ and $7{\cdot}9$; these parameter values were chosen to match conditions in concurrent experimental work. The downstream velocity profiles predicted by this numerical solution will be presented in § 8, where they will be compared with experimental data for these conditions and with the corresponding analytical solutions.

6. Elder's linearized theory applied to a partial screen

It was mentioned in the introduction that Elder (1959) believed his linearized theory could be applied to partial screens, providing $K \ll 1$. In order that this paper be as comprehensive as possible on the topic of partial screens, Elder's theory will be developed here for this case, and the results will be compared with the predictions of our source model and with the experimental data.

Elder's general solution for the velocity $U_{+\infty}$ downstream of a full screen of arbitrary shape and variable resistance is, in his notation,

$$U_{+\infty} - 1 = A(U_{-\infty} - 1) - \tfrac{1}{2}(1-A)\,S + EH.$$

When the upstream velocity $U_{-\infty}$ is uniform and the screen is plane, the relation reduces to

$$U_{+\infty}(y) = 1 - \tfrac{1}{2}(1-A)\,S + (2EBT/\pi)\ln\cot\tfrac{1}{2}\pi y,$$

where $T = \tan\alpha$; A, B and E are known algebraic functions of $K(y)$ and γ_0, and γ_0 and $S(y)$ are the mean value and deviation respectively of the effective pressure drop coefficient for a screen of variable resistance, as defined by

$$K\cos^2\alpha = \gamma_0(1+S).$$

Elder assumed that S was everywhere small, i.e. $S \ll 1$, in order to complete the linearization of the problem.

To apply the above results to a partial screen, the solidity of a full screen is considered to be discontinuous; that is, the screen has a non-zero coefficient K up to height λ and then K is assumed to be zero for the remainder. In this way

$$\gamma_0 = \lambda K\cos^2\alpha$$

and

$$S = \begin{cases} 1/\lambda - 1 & (0 \leqslant y < \lambda) \\ -1 & (\lambda < y \leqslant 1). \end{cases}$$

This of course means that $S \ll 1$ is no longer true. If this is disregarded in order to use the linearized equation, the far-downstream velocities are

$$u_2 = 1 - \tfrac{1}{2}(1-A)\,(1/\lambda - 1) + (2EBT/\pi)\ln\cot\tfrac{1}{2}\pi y,$$

$$u_3 = 1 + \tfrac{1}{2}(1-A) + (2EBT/\pi)\ln\cot\tfrac{1}{2}\pi y.$$

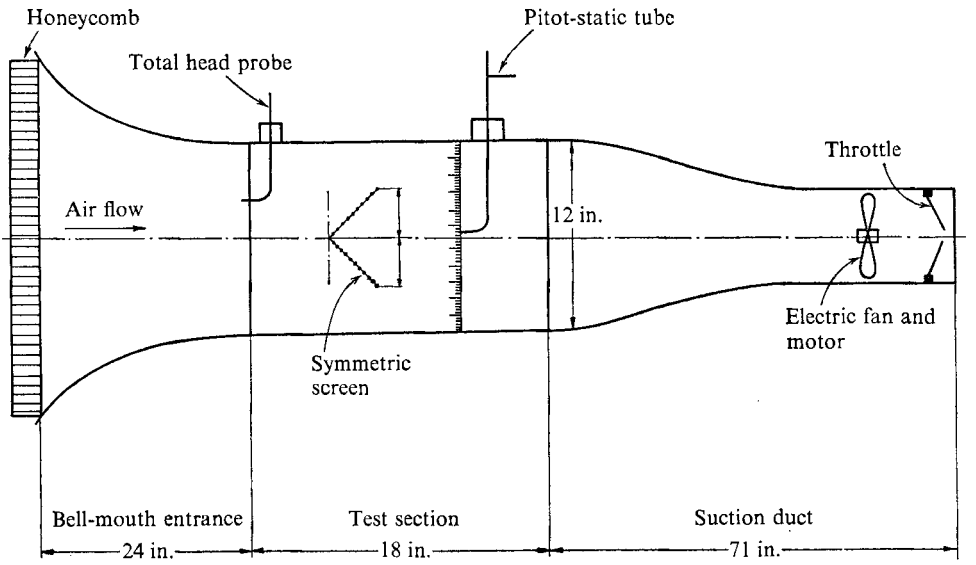

FIGURE 4. The wind tunnel used in the experiments. The rectangular test section has a width of 3 in. in the direction normal to this page.

7. Experiments

In order to assess the accuracy and range of validity of the mathematical model, as provided by the analytical and numerical solutions, a series of tests was conducted in a low-velocity wind tunnel. The experimental facility is shown schematically in figure 4. As indicated in the sketch, the screen configuration was symmetric about a horizontal centre-plane, thereby eliminating the boundary-layer effect of one wall, as well as doubling the working length of the test section and thus making it possible to measure the 'far-downstream' velocities within the 18 in. length of the section. Three different screens were used. Initial measurements with normal screens spanning the entire cross-section revealed that the minimum air speed above which all pressure drop coefficients were independent of velocity was 45 ft/s, consequently all tests were conducted with the free-stream velocity above this value. The test screens, which were half the height of the channel, had measured K values of 3·0, 4·6 and 7·9, and were inclined at angles of 0°, $\pm 30°$ and $\pm 45°$. For each combination of these two parameters, the downstream velocity distribution was measured using a stagnation-type tube, and the results are presented in the next section; the data will be given in terms of the normalized velocity $U_{+\infty}/U_{-\infty}$, where $U_{-\infty}$ is the uniform upstream velocity.

The wind tunnel was also appropriate in that the size of the mixing layer, the region between the wake and the external flow, was not large. Since the mathematical model is based on inviscid-flow theory, the solution generates two distinct downstream regions, with a step difference in velocity across the dividing streamline, as shown for example in figure 6. In a real viscous flow, the discontinuity is replaced by a mixing layer, the thickness of which has been established by

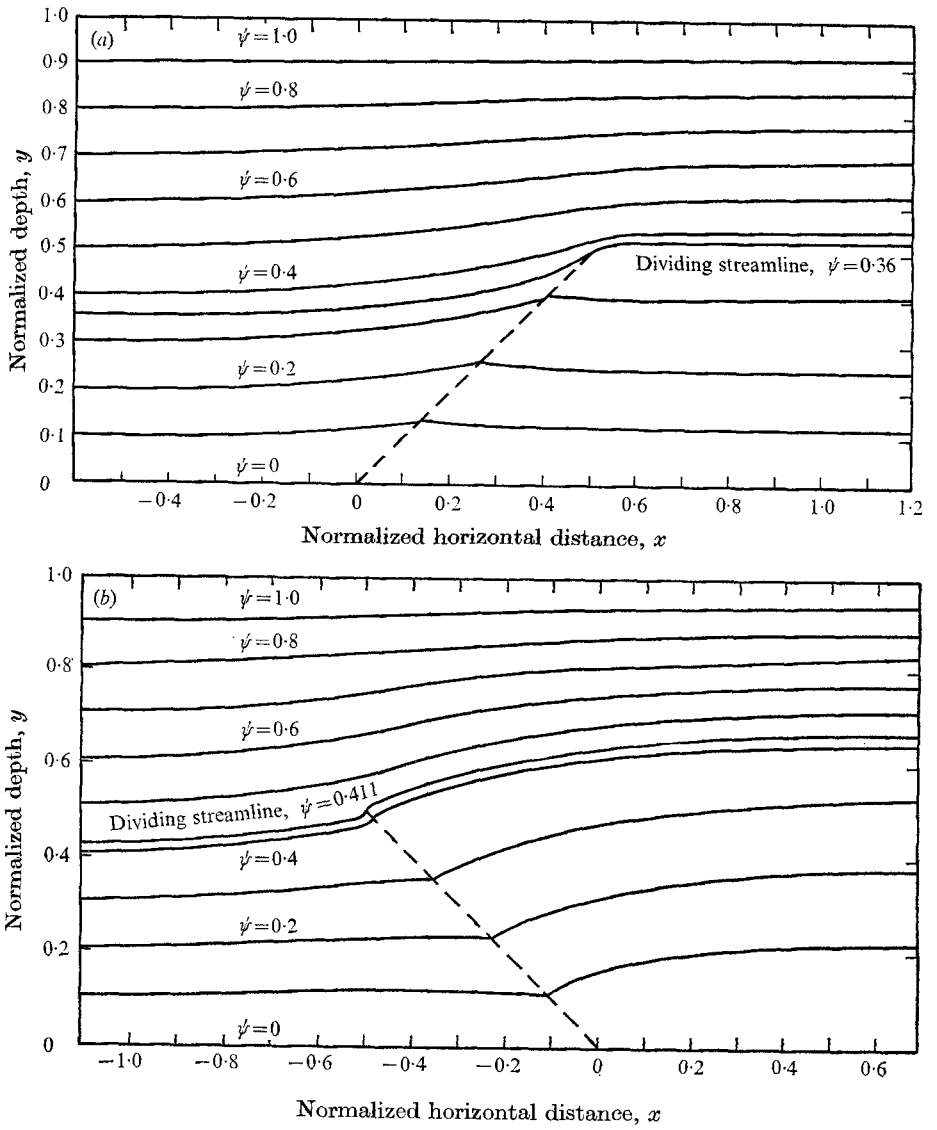

FIGURE 5. Streamline patterns predicted by the source model for (*a*) a low-solidity forward-tilting screen ($K = 3{\cdot}0, \alpha = 45°$) and (*b*) a high-solidity backward-tilting screen ($K = 7{\cdot}9$, $\alpha = -45°$).

theoretical and experimental methods (Görtler 1942). Letting x be the distance along the dividing streamline and y the distance normal to it, Görtler's paper shows that the local velocity in the mixing layer reaches 99 % of the external velocity at a distance $y = 0{\cdot}10x$. Calculations made with the present source model show that the downstream velocity distribution is within 1 % of its final profile at a downstream distance of one channel height, indicating that the mixing layer there should occupy no more than 20 % of the channel height. With viscous effects thus confined to a small region, the inviscid regions can be easily identified for comparisons with the theoretical predictions.

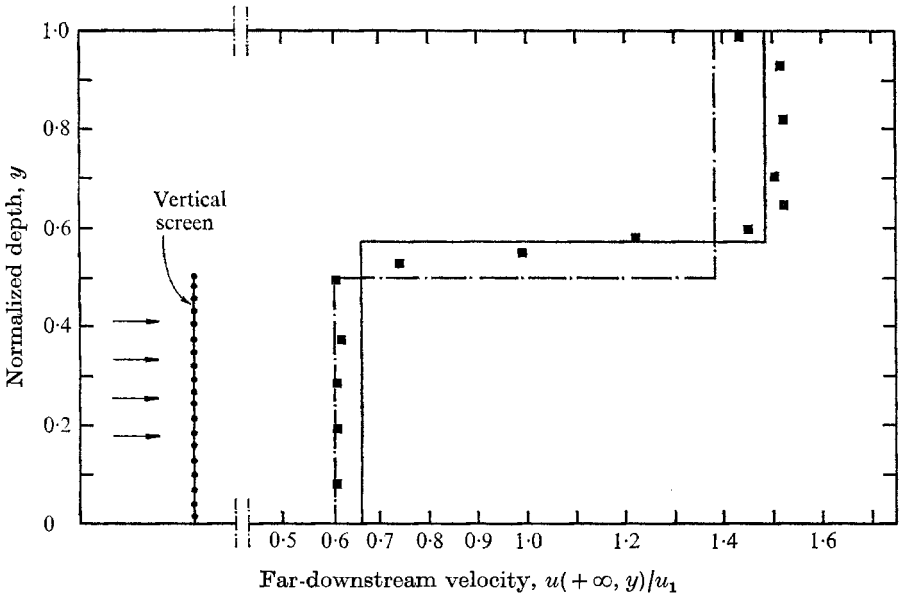

FIGURE 6. Typical experimental and analytical results for the velocity profile behind a normal (perpendicular) screen. $\lambda = 0{\cdot}5$, $K = 3{\cdot}0$. ■, experimental data; ——, analytical result, source model; —·—, Elder's linearized theory.

8. Results

Most of the results presented in this section are for the downstream velocity profile, as determined by experiment and as predicted by the analytical and numerical methods in §§5 and 6. Before showing these results, it might be informative to display typical streamline patterns generated by the source model; two such patterns are shown in figure 5, figure 5 (*a*) being for a low-solidity forward-tilting ($\alpha > 0$) screen and figure 5 (*b*) for a higher solidity, negatively inclined screen. Each pattern indicates the dividing streamline and the extent to which the streamlines are deflected by the screen.

Results for normal partial screens are presented in the next five graphs, figures 6–10. The results in figure 6 are for the typical screen conditions, $\lambda = 0{\cdot}5$ and $K = 3{\cdot}0$; the figure includes the experimental data, the velocity profile predicted by the analytical solution of the present model (§5.1) and also the profile predicted by Elder's linearized theory (§6). The experimental data in figure 6 indicate that the mixing layer occupies about 15 % of the channel height, in accordance with the estimate made earlier, and consequently the inviscid regions are easily distinguished.

To provide further comparisons between theory and experiment for a normal screen, the predicted and experimental values of the downstream velocities u_2 and u_3 were plotted for a range of K. The results for u_2 in figure 7 indicate that the source model is very accurate for K as high as 9. The predictions from Elder's theory indicate that his method is reliable for K at least up to one; K is not limited to values much less than one, as Elder presupposed. Figure 8 is a similar graph

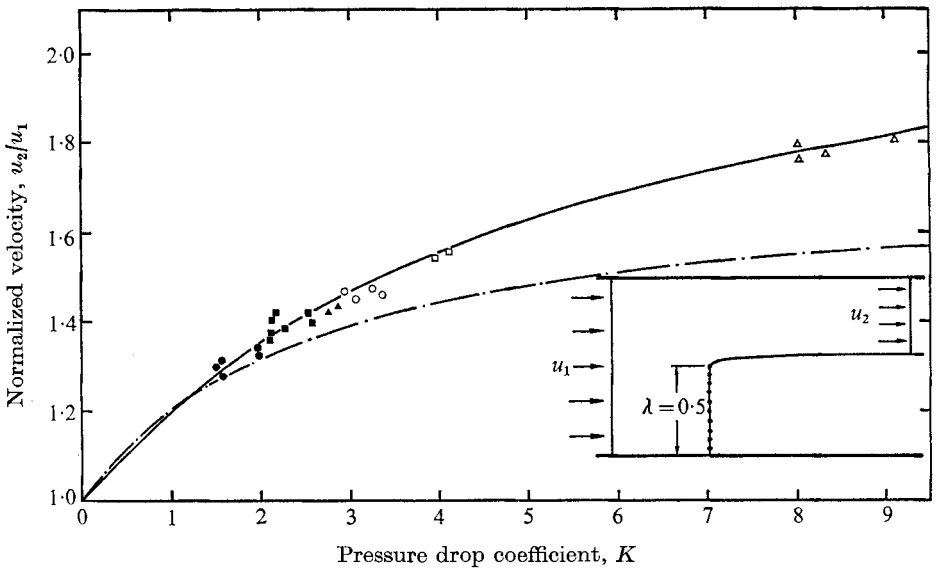

FIGURE 7. Analytical and experimental results for the free-stream velocity u_2 downstream of six normal screens as a function of the screen coefficient K. ——, analytical result, source model; —·—, Elder's linearized theory.

	●	■	▲	○	□	△
Number of mesh lengths per inch	20	18	24	40	30	30
Wire diameter (in.)	0·018	0·020	0·015	0·011	0·0135	0·0169
Material	Stainless steel	Stainless steel	Steel	Stainless steel	Steel	Steel

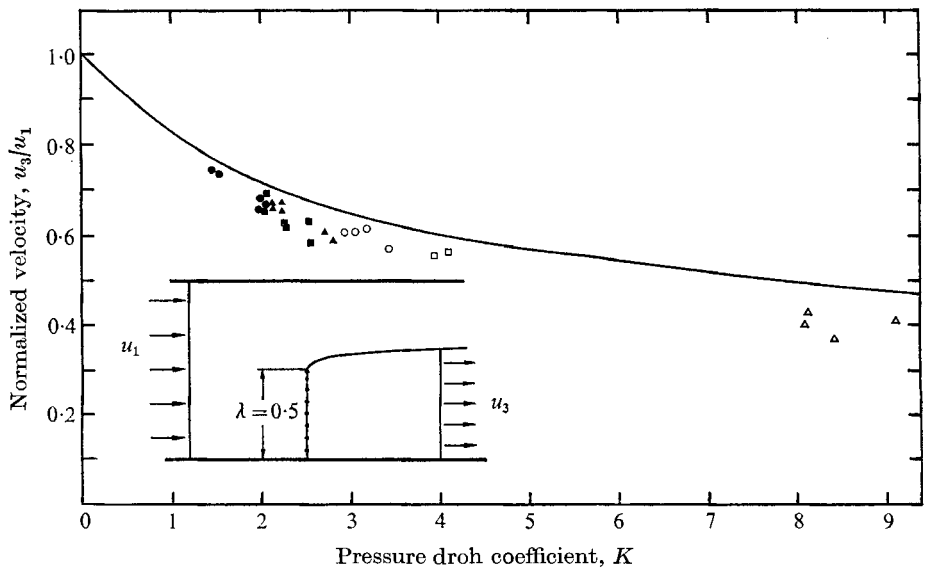

FIGURE 8. A comparison of analytical and experimental results for the wake velocity u_3 as a function of the screen coefficient K, for six normal screens. Notation as in figure 7.

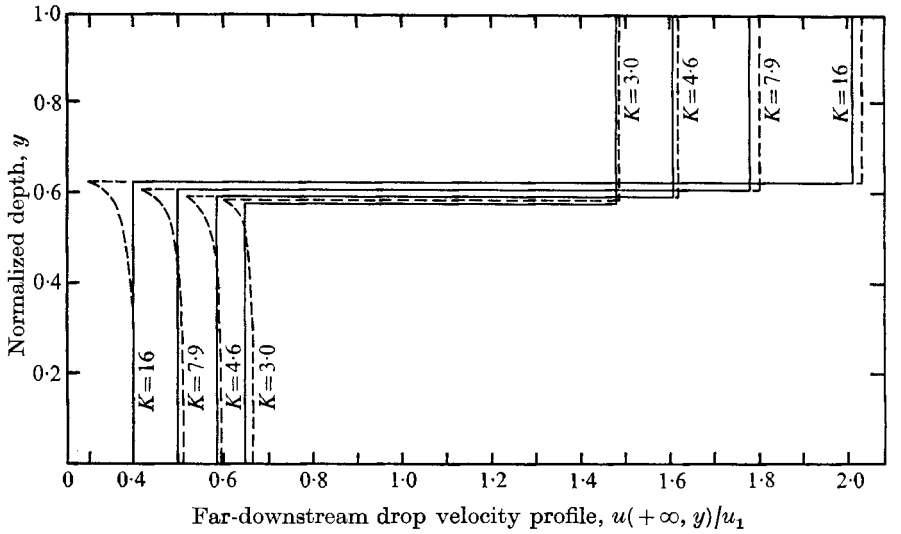

FIGURE 9. A comparison of analytical (solid line) and numerical (broken line) solutions of the present source model for the velocity distribution behind a normal screen; $\lambda = 0{\cdot}5$.

for the other downstream component u_3, and demonstrates a lack of agreement between the source model and experiment, a somewhat surprising discrepancy in view of the excellent agreement in figure 7. This lack of agreement, it was found, resulted from a shortcoming of the experiment and not the theory; more specifically, it was due to a boundary-layer effect downstream of the screen. This effect was in the form of a bulge in the velocity profile at the edge of the boundary layer, such that the local velocity was higher than the main-stream velocity: up to 10% higher, in fact. This phenomenon, which may be termed the bulge effect, has been thoroughly described by Lau & Baines (1968) in appendix B of their paper, and is expected when K is greater than one. One consequence of this excess velocity in the present work was a reduction in the mainstream velocity, since the total flow rate in the duct remained constant. This mechanism thus explains why the measured values for u_3 are below the theoretical curve in figure 8. It also accounts for the good agreement for the other downstream velocity u_2 in figure 7; the flow in this region did not pass through the screen and accordingly was not influenced by the bulge effect. There are additional ramifications of the bulge effect which affect subsequent data, and these will be discussed later in this section.

The analytical solution for a normal screen neglected the tangential velocities at the screen, and in order to assess the resulting error, the analytical results were compared with numerically computed results which included these terms. The comparison is shown in figure 9 for four values of K and demonstrates that the approximate solution given by the analysis provides an excellent estimate of the downstream velocity distribution; the major discrepancy is near the dividing streamline, but this is a minor concern since this part of the flow is a mixing layer for a real fluid, in which the velocity profile is continuous and not abrupt as shown. An important feature of figure 9 is that the velocity profile given by

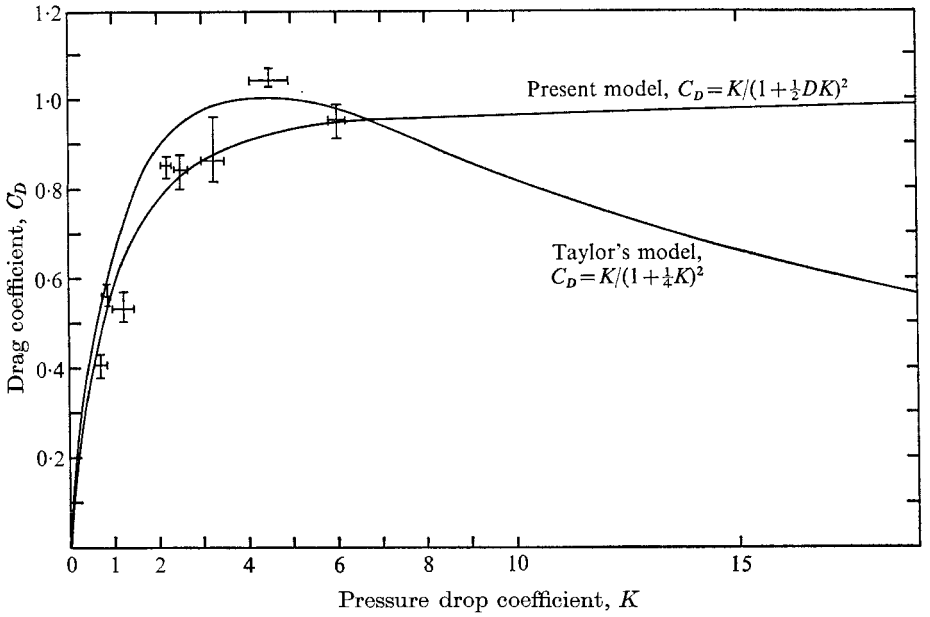

FIGURE 10. The drag coefficient of a plane screen normal to an infinite flow field ($\lambda \to 0$). ⊢⊣, experimental data of Taylor & Davies.

the numerical solution is uniform over most of the wake, showing that the approximate analytical solution, which yields a constant source strength and consequently a uniform downstream velocity, is indeed very accurate.

Since the present mathematical model has its origin in Taylor's (1963) source model, the results predicted by both models will be compared. As suggested earlier in § 5.1, this comparison will be in terms of the drag coefficient C_D for a two-dimensional screen in an infinite flow field. This corresponds to letting λ approach zero in our model, which from (9) predicts C_D to be $K/(1+\frac{1}{2}DK)^2$. This equation is compared with Taylor's result $C_D = K/(1+\frac{1}{4}K)^2$ and with experimental data obtained by Taylor & Davies (1963) in figure 10. The three results suggest that the present model is more accurate than Taylor's, especially for values of K above 1, notwithstanding the experimental point at $K \simeq 4{\cdot}5$. This point appears to be suspect, especially in relation to the next point, since the two suggest the unlikely result that C_D decreases as the solidity increases; it is much more reasonable that C_D increase monotonically with K, as the present model predicts.

Some typical results for inclined screens are presented in figures 11 (*a*) and (*b*) and figures 12 (*a*) and (*b*) each one showing, for a given set of experimental conditions, four downstream velocity profiles: (i) as measured, (ii) as predicted by an approximate solution of the source model, (iii) as given by a numerical solution and (iv) as predicted by Elder's linearized theory. The results in figures 11 and 12 were selected for presentation because they represent a wide variation in the experimental conditions; further results for intermediate conditions are available (Koo 1971), but these only confirm the trends illustrated in the four graphs and

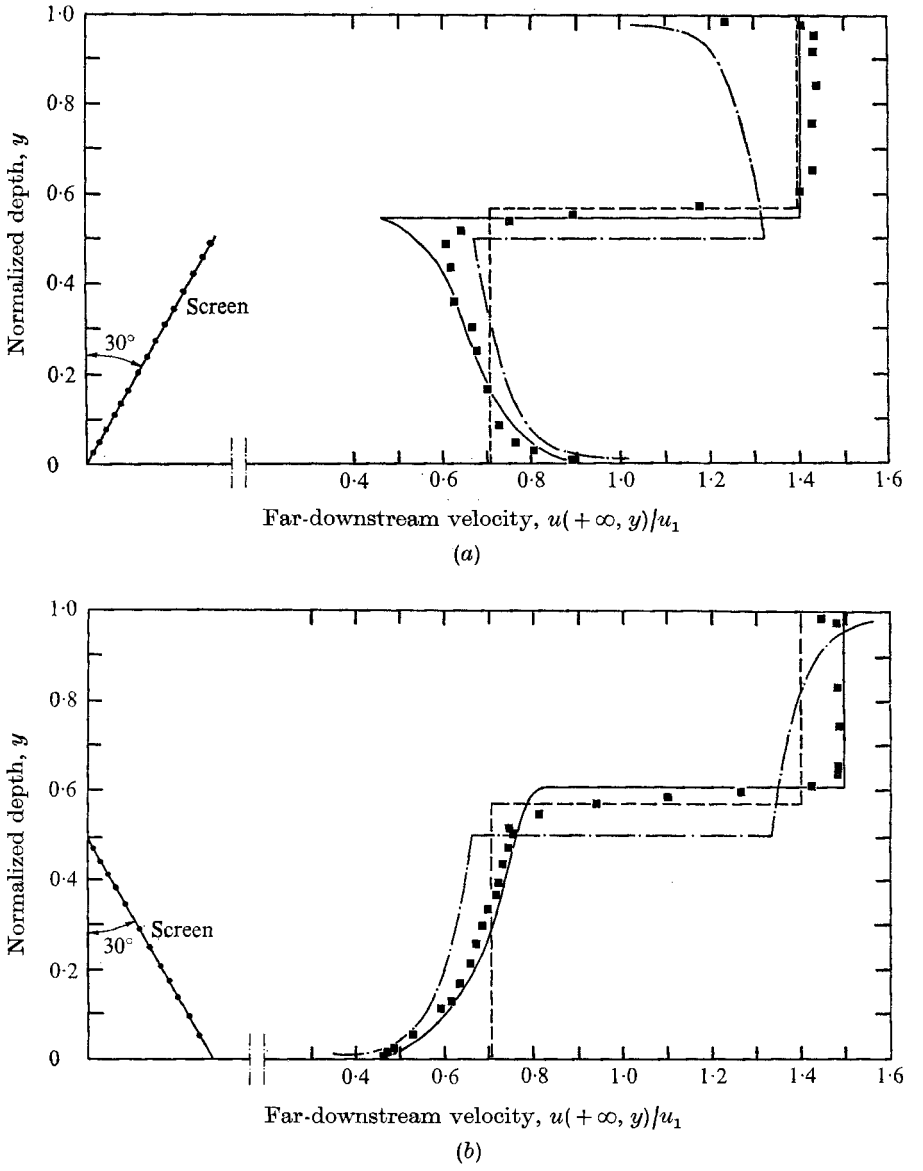

FIGURE 11. Analytical, numerical and experimental results for (*a*) a forward-tilted and (*b*) a backward-tilted screen of moderate solidity. – –, analytical solution of present model; —·—, Elder's linearized theory; ——, numerical solution of present model; ■, experimental data. $\lambda = 0{\cdot}5$, $K = 3{\cdot}0$. (*a*) $\alpha = 30°$. (*b*) $\alpha = -30°$.

therefore are not included here. The first two graphs, figures 11 (*a*) and (*b*), are for a low-solidity screen, $K = 3{\cdot}0$, at two moderate angles of inclination, $\alpha = \pm 30°$. Both figures show that the velocity predicted by the numerical solution is in excellent agreement with the experimental data. The two approximate solutions, cases (ii) and (iv), are generally within 10 %, which is reasonable since the flow distortion here is moderate. Elder's theory predicts the correct

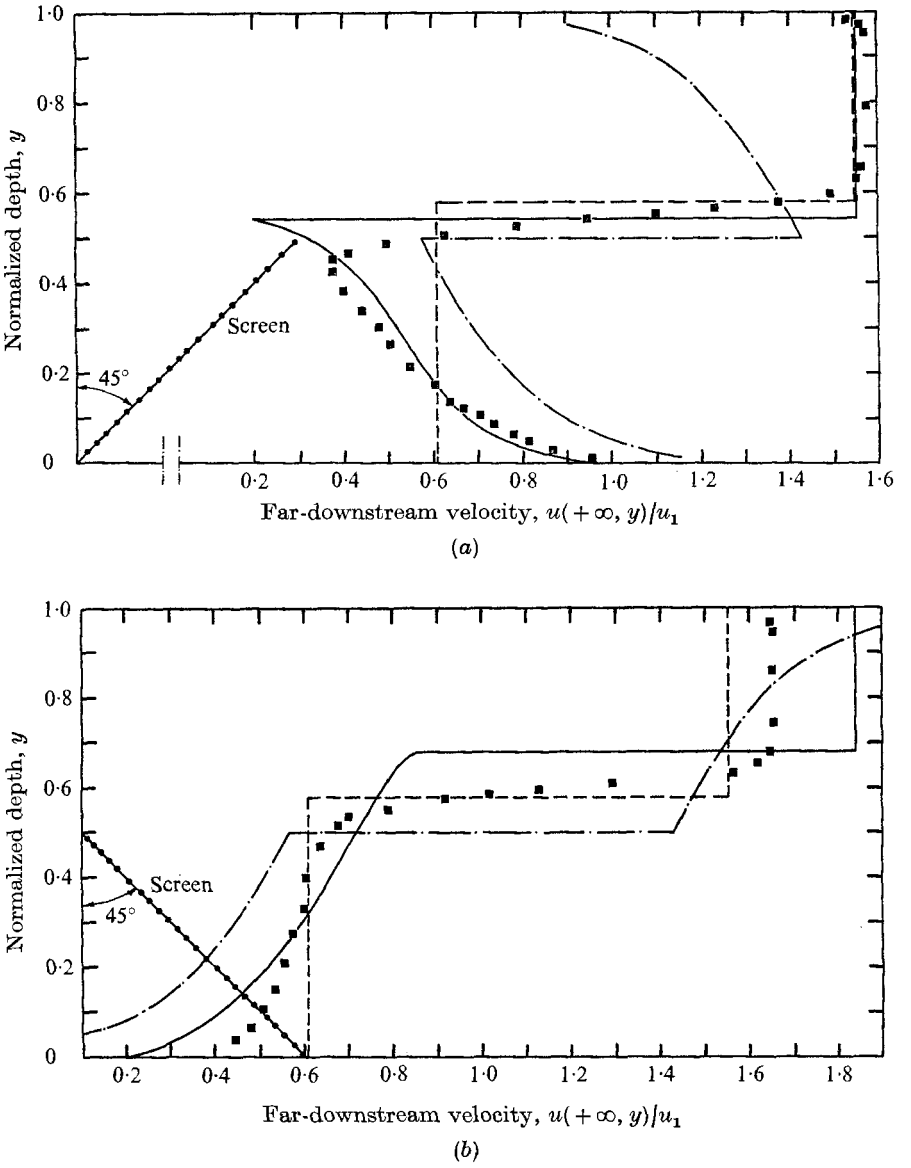

FIGURE 12. Analytical, numerical and experimental results for (*a*) a forward-tilted and (*b*) a backward-tilted screen of high solidity. $\lambda = 0{\cdot}5$, $K = 7{\cdot}9$. (*a*) $\alpha = 45°$. (*b*) $\alpha = -45°$. Other notation as in figure 11.

shape for the velocity profile in the wake but not in the external field, and the opposite is true for the analytical result. The analytical method, it will be remembered, yields a uniform velocity in the wake, which is proved in figures 11 (*a*) and (*b*) to be a good estimate of the average velocity for the actual distribution.

The results for the most extreme test conditions, $K = 7{\cdot}9$ and $\alpha = \pm 45°$, are shown in figures 12 (*a*) and (*b*). In the former, the agreement between the numerical

results and the experimental data is still good. The external velocity predicted by the analytical method is accurate, but the uniform wake velocity is no longer a suitable approximation to the actual profile. Also, Elder's solution is not a good approximation. In figure 12 (*b*), none of the predictions appears to be close to the experimental data. Actually, the numerical curve is considered to be the most reliable since the experimental data have been influenced significantly by the previously mentioned 'bulge effect'. The understanding of the bulge effect for this case requires a more thorough discussion than was presented earlier. In the boundary layer behind the screen, the pressure is larger than in the main flow and this difference can alter the flow in two possible ways. One consequence, as described earlier, is a bulge in the boundary-layer velocity profile accompanied by a velocity reduction in the core of the wake; the second is an increase in the average downstream pressure. The predominance of one of these consequences depends on the relative strength of the bulge effect along the length of the screen: that is, since the effect depends on Δp or $K\rho U_{\mathrm{I}}^2$, and since U_{I} varies along the screen, the effect varies along the screen. The effect at the tip is particularly important. For normal screens and for forward-leaning ones ($\alpha > 0$), the streamlines approach the screen most obliquely at the tip as shown in figure 5 (*a*), so that U_{I} and consequently the bulge effect is small there compared with that on the rest of the screen. Since the bulge effect for this case is confined to the core of the wake region, the first consequence dominates and the wake velocity is accordingly reduced. For a backward-leaning screen ($\alpha < 0$), the streamline pattern in figure 5(*b*) shows that the fluid passes obliquely through most of the screen, but not at the tip, where the flow is nearly normal. For this case, the maximum bulge effect is at the tip, and since the flow there is not confined as in the wake, the second consequence will predominate.This means that the average pressure just behind the screen tip is increased; this influence will be carried downstream, so that the pressure all along the dividing streamline is increased, including points far downstream. Consequently, by Bernoulli's equation, the external velocity u_2 will be reduced, as will the wake velocity u_3 near the dividing streamline; by continuity, u_3 in the remainder of the wake must increase. These changes in the downstream velocity distribution form precisely the pattern indicated in the comparison of the experimental and numerical data in figure 12 (*b*). Additional data for other backward-tilting screens showed the same pattern, with the discrepancy between the experimental and numerical results increasing with K and with the negative angle of the screen.

By considering special cases of the present source model, two further comparisons can be made between the model and previous work. When $\lambda \to 1$ and K is small, the situation represents a very porous screen across the full height of the channel. Elder's (1959) theory is particularly appropriate here and predicts the downstream velocity profile in terms of a universal co-ordinate containing the solidity of the screen and its angle of inclination. Since the results from our model cannot be expressed in terms of this universal co-ordinate, the comparison is made in figure 13 for two particular, but representative, cases: (*a*) $K = 2{\cdot}2$, $\alpha = 45°$ and (*b*) $K = 5{\cdot}2$, $\alpha = 30°$. The agreement in figure 13 is very good, reconfirming the validity of the source model at low values of K. At the other

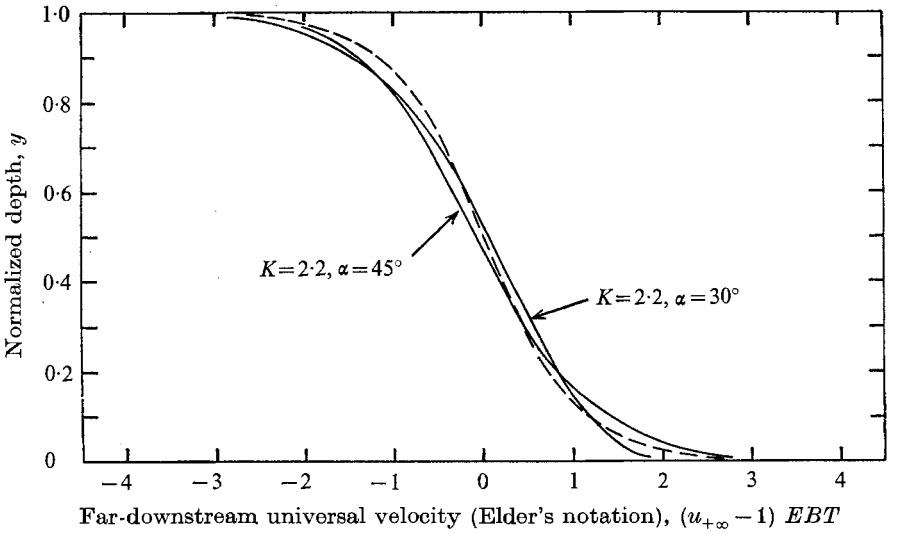

FIGURE 13. The downstream velocity distribution predicted by the present model (solid line) and by Elder's linearized theory (broken line) for the case of a full screen, $\lambda = 1$.

extreme $K \to \infty$, the screen becomes impermeable, and it is then necessary to compare the results predicted by the present model with those given by free-streamline theory for a plate attached to the channel wall, i.e. for a two-dimensional orifice. This comparison is provided in figure 14 for three angles of inclination and for the full range of screen heights. The agreement is marginally satisfactory for the normal screen and perhaps for the forward-leaning one; this result, along with the previous results for finite values of K, suggests that the present mathematical model is useful for screens of high solidity, but that it cannot be extended to the limiting case $K \to \infty$.

9. Discussion and conclusions

It appears that the source model proposed in this paper accurately represents the two-dimensional flow around and through a screen, judging by the agreement of the experimental data with numerical solutions of the model. The experimental facility was not adequate to determine fully the region of validity for the model, but the data suggest that the solutions are accurate for screens of all heights and with K values as high as 10, perhaps higher. An approximate analytical solution of the model provides results which are algebraic and therefore easily applied; in this analysis, the vertical velocity at the screen may be ignored for certain screen conditions, which results in a uniform source strength along the screen and consequently a straightforward algebraic solution. The comparison of this solution with the numerical solution and experimental results indicates that this approximation is excellent for normal screens and useful for forward-leaning ones.

The major shortcoming of the model is the unsatisfied deflexion condition at the screen. As mentioned previously, there are not enough unknowns in the

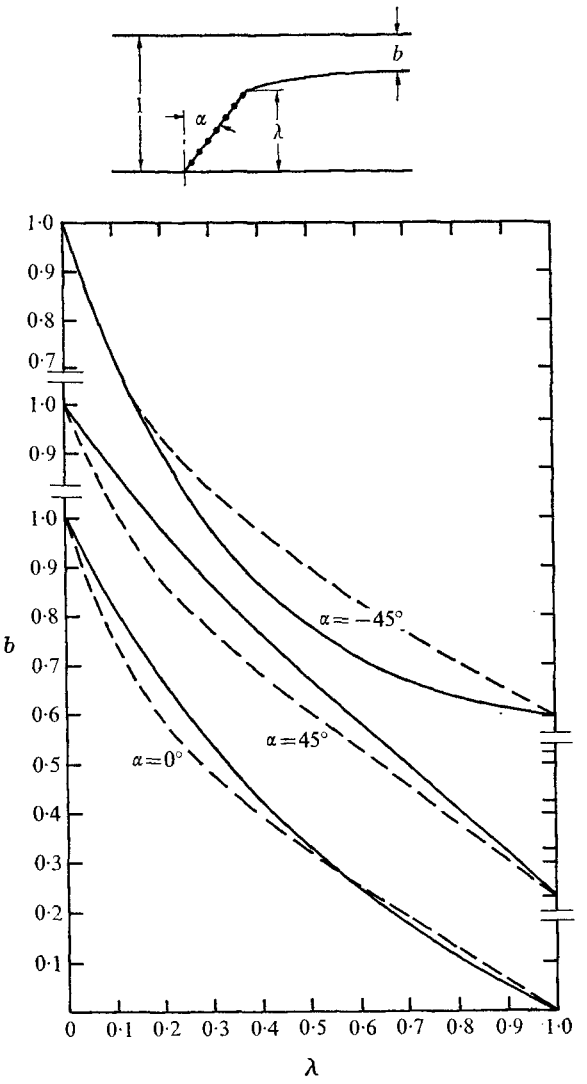

FIGURE 14. Comparison of the results from free-streamline theory (broken line) with those from the present model (solid line) when the screen solidity becomes infinite, $K \to \infty$.

problem to meet this matching condition as well. Yet the model, as it is, predicts deflexions of the right order of magnitude. For normal screens, (5) reveals that E is equivalent to the deflexion coefficient D_θ. When Γ in (7) is constant and set equal to $2DK/(2+DK)$ as before, then E becomes $(1+DK)^{-1}$, which is a good approximation of the formula $D_\theta = 1{\cdot}1/(1+K)^{\frac{1}{2}}$ for values of K up to 5. Koo (1971) has shown that the equivalence of E and D_θ holds for inclined screens as well, and consequently E may be compared to D_θ calculated from Taylor & Batchelor's formula given in the introduction. This comparison has been carried out for a variety of cases in Koo's thesis and shows that $E(\eta)$ not only has the same behaviour as $D_\theta(\eta)$, but is often numerically close to D_θ as well. Hence the

present model, without further modifications, roughly satisfied the deflexion condition at the screen.

Some further insight about the model may be gained by integrating the differential equation which defines E in § 5.1; this procedure shows that B is related to E, or equivalently to D_θ, by

$$B(\psi) = \psi^{-1} \int_0^\psi E(\xi)\, d\xi.$$

When E is constant or approximately so, as in the analytical solutions, then $B = E$, and consequently a simple interpretation of B is that it is equivalent to the deflexion coefficient.

A more refined mathematical model was attempted by adding a vortex distribution to the source distribution along the screen. In pursuing a numerical solution it was found that the iterations did not converge for some cases, and for the well-behaved cases the vortex strength was about one-tenth of the source strength and consequently had little effect on the flow. Since the improvement in accuracy was minimal, the addition of a vortex distribution is not considered worthwhile.

It should be pointed out that our proposed mathematical model is useful for more general situations. This paper has fully explored the model for the situation of a plane screen of uniform solidity in a channel with an approaching two-dimensional uniform flow, and it may be apparent that other situations can be treated using the model, though generally not with analytical methods. The following variations are possible, providing changes are made in the analysis as noted: (*a*) a screen of arbitrary shape can be dealt with straightforwardly by including $g(\eta)$ in the general equations for u_I and v_I [thus revising $H(x, y, \eta)$ and $P(x, y, \eta)$], and by noting that the inclination of the screen is a local property, i.e. $\alpha = \alpha(\eta)$; (*b*) a screen of non-uniform solidity requires that the two matching conditions be revised to allow $K = K(\eta)$; (*c*) a non-uniform upstream velocity distribution can be treated by including $u_1(\psi)$ in the second matching condition (it cancels out for uniform flow) and by noting that u_2 is no longer a constant, i.e. $u_2 = u_2(\psi)$. These three cases, or any combination of them, can be treated by the present numerical method with some slight modifications to the computer program. It may be apparent that the present source model can also be applied to some three-dimensional problems. If a finite screen is located in a semi-infinite flow field, then a solution of the flow field is possible, using in this case three-dimensional potential theory, and not functions of a complex variable.

The authors are grateful for the financial support of this research by the National Research Council of Canada, and for the help given by W. Douglas Baines, who proposed the problem and encouraged the work throughout.

Appendix. Determining the horizontal velocity at the screen

Section 5.1 shows that, for a normal screen, the horizontal velocity is

$$u_\mathrm{I}(x, y) = 1 + \int_0^\lambda \Gamma(\eta)\, H(x, y, \eta)\, d\eta,$$

where

$$H(x,y,\eta) = \frac{1}{4}\left[\frac{\sinh \pi x}{\cosh \pi x - \cos \pi(y-\eta)} + \frac{\sinh \pi x}{\cosh \pi x - \cos \pi(y+\eta)}\right].$$

On the screen, where $x \to 0$, $H(0,y,\eta) \to 0$ providing $\eta \neq y$. (We need not worry about the other singularity $\eta = -y$ since η is restricted to the interval $(0,\lambda)$ for this function.) At the point $\eta = y$, L'Hopital's rule shows that

$$\lim_{\substack{x \to \pm 0 \\ \eta \to y}} H(x,y,\eta) \to \pm \infty.$$

Consequently $H(0,y,\eta)$ becomes an impulse function of the form $\pm A\ \delta(y-\eta)$, where the notation $\pm$ is used to indicate whether the screen is approached from the right $(+)$ or left $(-)$. To characterize $H(0,y,\eta)$ fully, the constant A must be determined, and this can be accomplished by finding the integral of the first term of H, i.e. finding

$$I = \lim_{x \to 0} \frac{1}{4}\int_a^b \frac{\sinh \pi x}{\cosh \pi x - \cos \pi(y-\eta)}\, d\eta,$$

where the interval (a,b) includes the point $\eta = y$. The second term in H does not contribute since it is identically zero when $x = 0$. By using the following indefinite integral, which is not well known but which can be verified straightforwardly by differentiation,

$$\int \frac{\sinh \pi x}{\cosh \pi x - \cos \pi(y-\eta)}\, d(\tfrac{1}{2}\pi\eta) = \tan^{-1}\left\{\frac{\tanh \frac{1}{2}\pi x}{\tan[\frac{1}{2}\pi(y-\eta)]}\right\}$$

it follows that

$$2\pi I = \tan^{-1}\left\{\frac{\tanh \frac{1}{2}\pi x}{\tan[\frac{1}{2}\pi(y-b)]}\right\} - \tan^{-1}\left\{\frac{\tanh \frac{1}{2}\pi x}{\tan[\frac{1}{2}\pi(y-a)]}\right\}.$$

As $x \to 0+$,

$$2\pi I \to \tan^{-1}\left\{\frac{0+}{-1}\right\} - \tan^{-1}\left\{\frac{0+}{+1}\right\}$$

$$= \tan^{-1}(0-) - \tan^{-1}(0+);$$

similarly, as $x \to 0-$,

$$2\pi I = \tan^{-1}(0+) - \tan^{-1}(0-).$$

The argument for the tangent function is assumed to have an interval of 2π, say from $-\pi$ to π, and thus the value of $\tan^{-1}(0+)$ may be 0 or $-\pi$, corresponding to the first and third quadrants; likewise for $\tan(0-)$, the choice is $+\pi$ or 0, corresponding to the second and fourth quadrants. The choice of values for $\tan^{-1}(0+)$ and $\tan^{-1}(0-)$ appears somewhat arbitrary, but must be consistent with the physics of the situation. Since the integral I cannot be zero, $\tan^{-1}(0+)$ and $\tan^{-1}(0-)$ cannot simultaneously be zero. The two possible solutions then are $\tan^{-1}(0-) = 0$, $\tan^{-1}(0+) = -\pi$ and $\tan^{-1}(0-) = \pi$, $\tan^{-1}(0+) = 0$. Both solutions, however, give the same values for I, namely

$$I(x \to 0\pm) = \pm \tfrac{1}{2}.$$

Therefore

$$\lim_{x \to 0\pm} H(x,y,\eta) = \pm \tfrac{1}{2}\delta(y-\eta).$$

Consequently,

$$U_{\mathrm{I}} = u_{\mathrm{I}}(0-, y) = 1 + \int_0^{\lambda} \Gamma(\eta)\, H(0-, y, \eta)\, d\eta$$
$$= 1 - \frac{1}{2}\int_0^{\lambda} \Gamma(\eta)\, \delta(y-\eta)\, d\eta$$
$$= 1 - \tfrac{1}{2}\Gamma(y)$$

and
$$U_{\mathrm{II}} = E(\psi)\, u_{\mathrm{I}}(0+, y) = E\left[1 + \frac{1}{2}\int_0^{\lambda} \Gamma(\eta)\, H(0+, y, \eta)\, d\eta\right]$$
$$= E[1 + \tfrac{1}{2}\Gamma(y)].$$

REFERENCES

Baines, W. D. & Peterson, E. G. 1951 *Trans. A.S.M.E.* **73**, 467–480.

Elder, J. W. 1959 *J. Fluid Mech.* **5**, 355–368.

Görtler, H. 1942 *Z. angew. Math. Mech.* **22**, 244.

Koo, J.-K. 1971 Ph.D. thesis, University of Toronto.

Küchemann, D. & Weber, J. 1953 *Aerodynamics of Propulsion*, chap. 3. McGraw-Hill.

Lau, Y. L. & Baines, W. D. 1968 *J. Fluid Mech.* **33**, 721–738.

Robertson, J. M. 1965 *Hydrodynamics in Theory and Application*. Prentice-Hall.

Schubauer, G. B., Spangenberg, W. G. & Klebanoff, P. S. 1950 *N.A.C.A. Tech. Note*, no. 2001.

Taylor, G. I. 1963 In *The Scientific Papers of G. I. Taylor*, vol. 3, pp. 383–386. Cambridge University Press.

Taylor, G. I. & Batchelor, G. K. 1949 *Quart. J. Mech. Appl. Math.* **2**, 1–28.

Taylor, G. I. & Davies, R. M. 1963 In *The Scientific Papers of G. I. Taylor*, vol. 3, pp. 391–405. Cambridge University Press.